Chapter 3

Experimental optical techniques and theory

3-1 Raman-scattering setup

Raman effect had been predicted by Smekal in 1923,[61] however, Raman scattering was first observed by Raman and Krishnan five years later in 1928.[62] This remarkable work helped Raman won the Nobel Prize in Physics in 1930. Raman-scattering process mainly probes the phonons in the frequency range between 100 and 1000 cm^{-1}. According to its particular process of how photons interacting with materials, Raman-scattering measurements provide not only information of lattice vibration but also the excitations of the charge, spin, and orbital degrees of freedom.

When the photons are scattered by matter, there are three types of linear responses. First, it could be absorbed. The photon releases all its energy to excite various processes in the solids. Second, the elastic scattering could happen. In this case, the incident photon may change its direction of propagation but suffer no energy loss. When the incident light with wavelength close to lattice constant, such scattering is named Bragg scattering, for example X-ray scattering. If the wavelength of incident light is much longer than lattice constant, this scattering is called Rayleigh scattering which is always seen at the position without energy shift in the Raman scattering spectrum. Third, the photons may undergo the inelastic scattering, Raman scattering. The scattering can be described with three processes: (i) the incident laser photon ($\hbar\omega_l$)

is virtually absorbed by solid then creates an electron-hole pair; (ii) the electron or hole scatters, creating or annihilating an elementary excitation such as phonon, plasmon, and magnon, which has energy ($\hbar\omega_0$); and (iii) the electron-hole pair recombines, emitting radiation of energy ($\hbar\omega_S$). Since the conservation of energy is still valid, the relation of these frequencies is:

$$\omega_S = \omega_I \pm \omega_0 \ .$$

(3.1.1)

The minus sign refers to the Stokes process, corresponding to the creation of an excitation. On the other hand, the plus sign refers to the Anti-Stokes process, corresponding to annihilate an excitation. An idealized theoretical model of Rayleigh scattering and Stokes and anti-Stokes Raman scattering is shown in Fig. 3 - 1. Besides, Fig. 3 - 2[63] shows a Stokes and anti-Stokes Raman spectra of carbontetrachloride, displaying the symmetry of wavenumber shift about the Rayleigh scattering peak. We can also observe that the intensity of anti-Stokes mode is much weaker than the Stokes mode, because that the photons creating a phonon and losing energy is easily than annihilating a phonon and getting energy.

The many-particle theory is a good tool to deal with the Raman spectra line-shape. In the case of the optical phonons and polaritons, the spectra line-shape is described with correlation function $A_l^u(q,\omega)$, which is given by S. Barker:[64]

$$A_l^u(0,\omega) = (\bar{n}(\omega)+1)\left|\bar{u}_l(\omega)_l\right|^2 \frac{2}{\pi} \frac{\omega_l\omega\gamma_l}{(\omega_l^2 - \omega^2)^2 + \omega^2\gamma_l^2}$$
$$\bar{n}(\omega) = \frac{1}{e^{\hbar\omega/k_BT}-1}$$

(3.1.2)

where $\bar{u}_l(\omega)_l$ is the amplitude of the lth normal mode. ω_l and γ_l represent the normal frequency and phenomenological damping constant of the lth normal mode. Consider the amplitude is independent of frequency in a small frequency range, Eq. (3.1.2) can

be simplified as:

$$A_l''(0,\omega) = (\frac{1}{e^{\hbar\omega/k_BT} - 1} + 1) A_l^2 \frac{\omega\gamma_l}{(\omega_l^2 - \omega^2)^2 + \omega^2\gamma_l^2} \quad . \tag{3.1.3}$$

This formula is similar with the peak-shape Lorentz model. Therefore, we analyze the Raman spectra with Lorentz profile basically.[65]

Moreover, to determine where the vibration is active in the Raman spectrum, the selection rules must be applied to its normal vibration. The cross section σ of Raman scattering can be presented as:

$$\sigma = A \left| e_S^i \chi^{ij} e_I^j \right|^2, \tag{3.1.4}$$

where A is a constant, χ^{ij} are the second order susceptibilities which are restricted by the symmetric properties, and e_S^i and e_I^i are the units parallel to the electric fields of scattering and incident laser, respectively. For our samples, the hexagonal crystal structure of Na_xCoO_2 consisting of CoO_2 and Na layers parallel to the ab - planes belongs to space group D_{6h} ($P6_3/mmc$, $Z = 2$). As described in previous papers,[23,48] there are five Raman active phonon modes: $A_{1g} + E_{1g} + 3E_{2g}$. These five modes can be identified unambiguously by specific polarization configurations. Their second order susceptibilities are restricted by the symmetric properties:[66]

$$\chi(A_{1g}) = \begin{bmatrix} a & 0 & 0 \\ 0 & a & 0 \\ 0 & 0 & b \end{bmatrix},$$

$$\chi(E_{1g}) = \begin{bmatrix} 0 & 0 & -d \\ 0 & 0 & d \\ -e & e & 0 \end{bmatrix},$$

$$\chi(E_{2g}) = \begin{bmatrix} f & f & 0 \\ f & -f & 0 \\ 0 & 0 & 0 \end{bmatrix},$$
(3.1.5)

where the letters indicate the nonzero components. This information will help us to analyze the polarized Raman spectra so that we can get correct Raman phonon assignment.

We used three sets of micro-Raman instruments in this study. Our Raman scattering spectra with 514.5 laser line at room temperature were mainly taken in Tatung University. Whereat the RENISHAW inVia Raman Microscope 1000 single monochromator equipped with 1800 grooves/mm grating and a thermoelectric cooled Renishaw's RenCam charge-coupled detector (CCD) were used. The sketch of the optical setup of micro-Raman scattering is shown in Fig. 3 - 3, while the schematic diagram of a single monochromator is shown in Fig. 3 - 4. Moreover, the spacial resolution in the spectroscopy was about 2 ~ 3 μm under the 50× objective and the laser power was controlled within 5 mw in case the sample was burned by excess laser power.

We also performed micro Raman-scattering measurements with 632 nm laser source. These spectra were taken in Research Center for Applied Sciences in Academia Sinica. Where the Horiba Jobin Yvon LabRAM HR-800 equipped with 1200 grooves/mm grating and a liquid-nitrogen cooled and 1024 pixel wide charge-coupled detector (CCD) were used. The spacial resolution in the spectroscopy was about 2 ~ 3 μm under the 100× objective and the laser power was controlled within 5 mw in case the sample was burned by excess laser power. The optical resolution is 0.5 ~ 0.6 cm^{-1} within 70 ~ 1000 cm^{-1} frequency range.

Moreover, our temperature-dependent Raman-scattering measurement was taken

with 514.5 nm laser line in NTNU. Where the Dilor XY 800 triple monochromator equipped with 1800 grooves/mm grating and a liquid-nitrogen cooled and 1024×512 pixel wide charge-coupled detector (CCD) were used. The sketch of the optical setup of micro-Raman scattering is shown in Fig. 3 - 5, while the schematic diagram of a single monochromator is shown in Fig. 3 - 6. Moreover, there is a cooling system equipped on the Raman spectrometer with a continuous flow helium cryostat is used. The cooling setup is shown in Fig. 3 - 7.[67]

3-2 Optical spectrometers

A vacuum Fourier transform infrared spectrometer (Bruker IFS 66v/s) was used for the far-infrared (FIR: 50 ~ 650 cm^{-1}) and middle infrared (MIR: 370 ~ 6000 cm^{-1}) measurements. In order to obtain high-solution optical spectra, FTIR spectrometer was constructed based on the Michelson interferometer.[65] Figure 3 - 8 illustrates the experimental setup of the FTIR spectrometer. It is composed of two light sources, beam splitters, and detectors, which can be changed under the computer control. In FIR region, a mercury light setting, a multilayer T222 beam-splitter, and a Si bolometer were used; in MIR region, a Golbar light, a KBr T301 beam-splitter, and a deuterated triglycine sulfate (DTGS D301) were used. We use the near-normal incidence (the angle between incident ray and reflected ray is less than 11°) configuration. In order to collect the correct reflectance spectra data, we used gold mirrors as a reference in our FIR and MIR measurements due the near 100% reflectance in FIR and MIR regions of gold mirrors. After use the reflectivity of gold in the textbook, the correct measured reflectance spectra R_{exp} are obtained by the

$$R_{sample} = \frac{R_{sample}^{measured}}{R_{Au}^{measured}} \times R_{Au}^{textbook}. \qquad (3.2.1)$$

Moreover, PerkinElmer Lambda 900 is a high-energy system that enables spectral recording from 3850 to 55000 cm^{-1}. Figure 3 - 9 presents the experimental setup of the Lambda 900 spectrometer. It contains double-beam and double-monochromator (grating-type) spectrophotometer with holographic gratings, large collimating mirrors and computer-controlled synchronized slit mechanisms. The grating-type monochromator is composed of an entrance slit, a grating, and an exit slit, which is suitable for medium or high resolution in comparison with a prism-type monochromator.[69] Double-monochromator has two principle advantages: including (a) it can decrease the value of stray radiation to 0.00008% in comparison with 0.01 of single monochromator (stray radiation may originate from the specimen holder, or from parts of the instruments.), and (b) it can provide more accurate wave length. After passing through the double-monochromator, beam light certainly decrease its intensity. So that, a chopper was used to change the path of light, which is in order to reduce uncertainties that are caused by the lower intensity of light. In near-infrared (NIR) and visible (VIS) region, the tungsten lamp and photoconducting detector were used. In ultraviolet (UV) region, the deuterium lamp and photomultiplier tube were used. In order to collect the correct reflectance spectra data, we used Al mirrors as a reference in our measurements.

A continuous flow helium cryostat is used to provide the low-temperature infrared spectra measurements. Figure 3 - 10 illustrates the experimental setup of the cooling system. The experimental setup provides the measurements at the temperature range from 10 K to 340 K.[68]
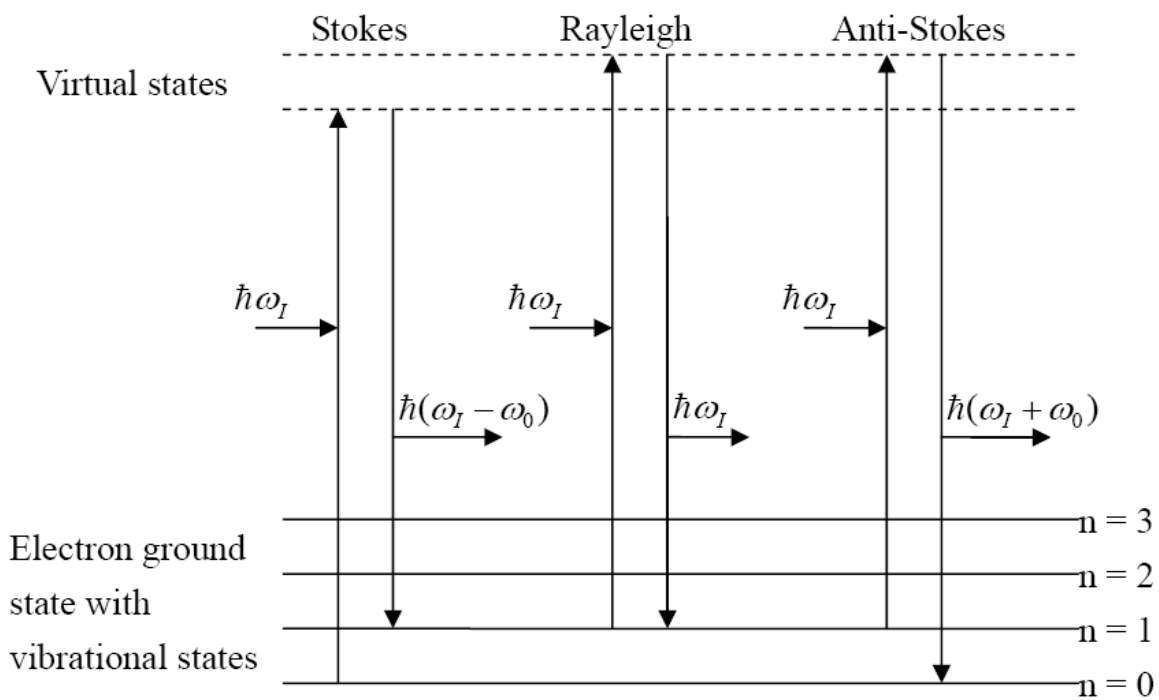
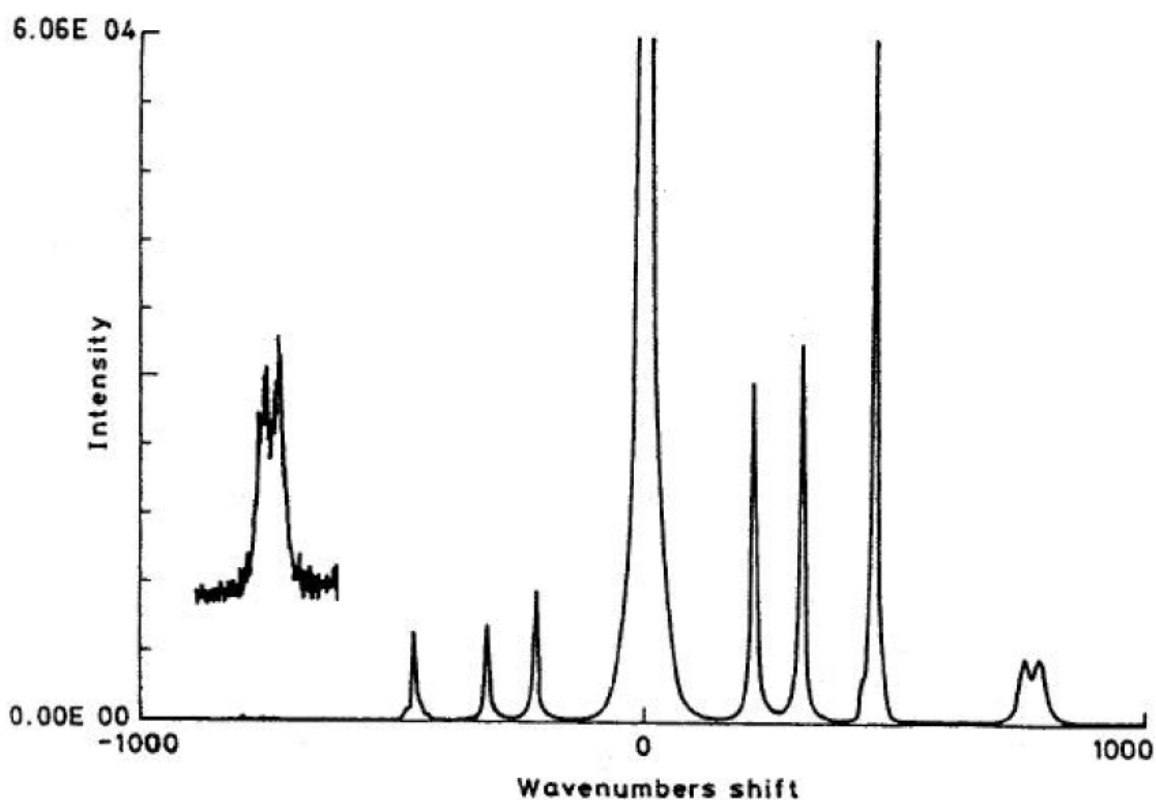Fig. 3 - 1. Idealized theory model of the Rayleigh scattering, Stokes and anti-Stokes Raman scattering.

Fig. 3 - 2. Stokes and anti-Stokes Raman spectra of carbontetrachloride.[63]
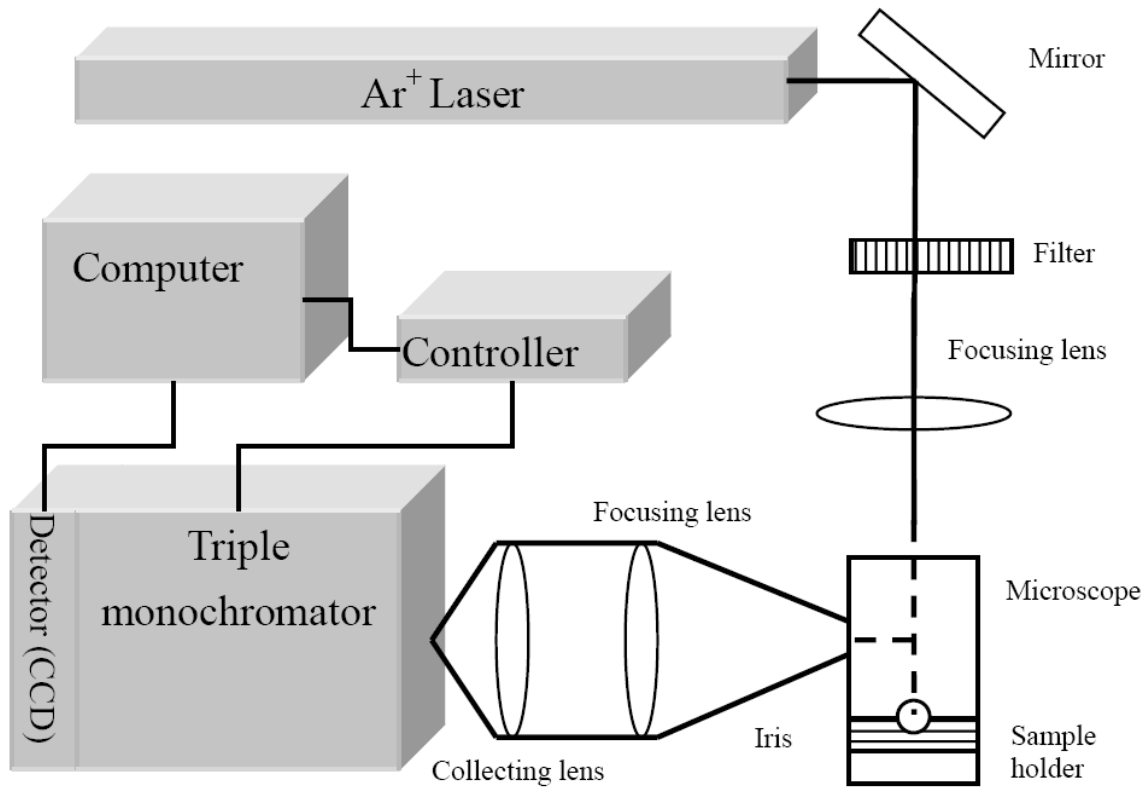
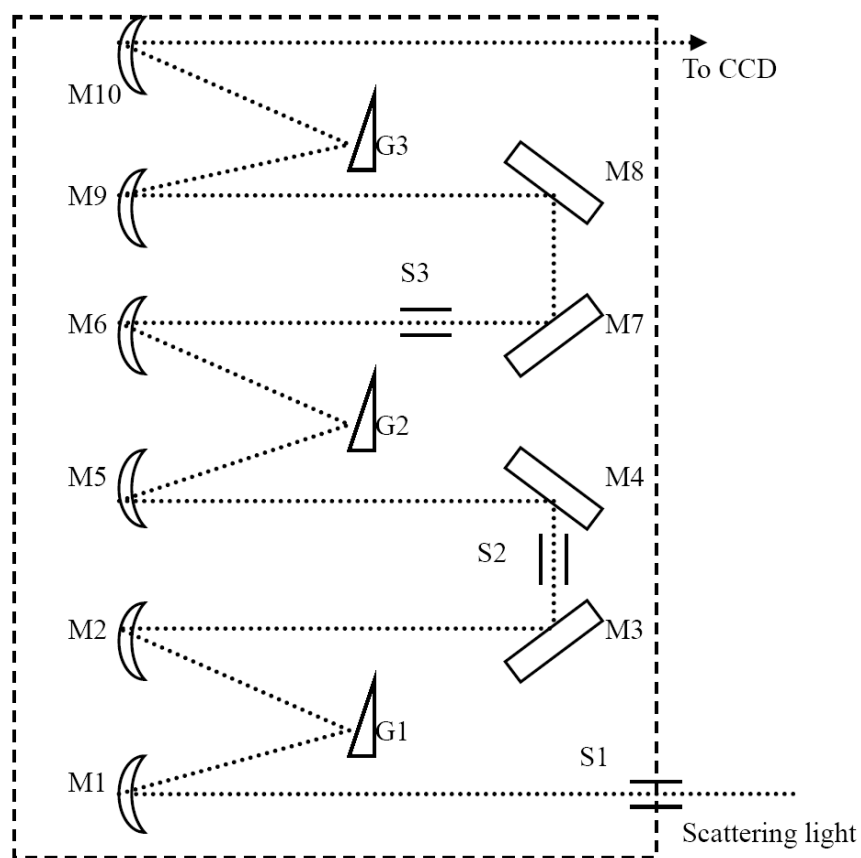Fig. 3 - 3. A sketch of the setup of the micro-Raman scattering in NTNU.

Fig. 3 - 4. Schematic diagram of a triple monochromator. G is optical grating, M is mirror, and S is slit.
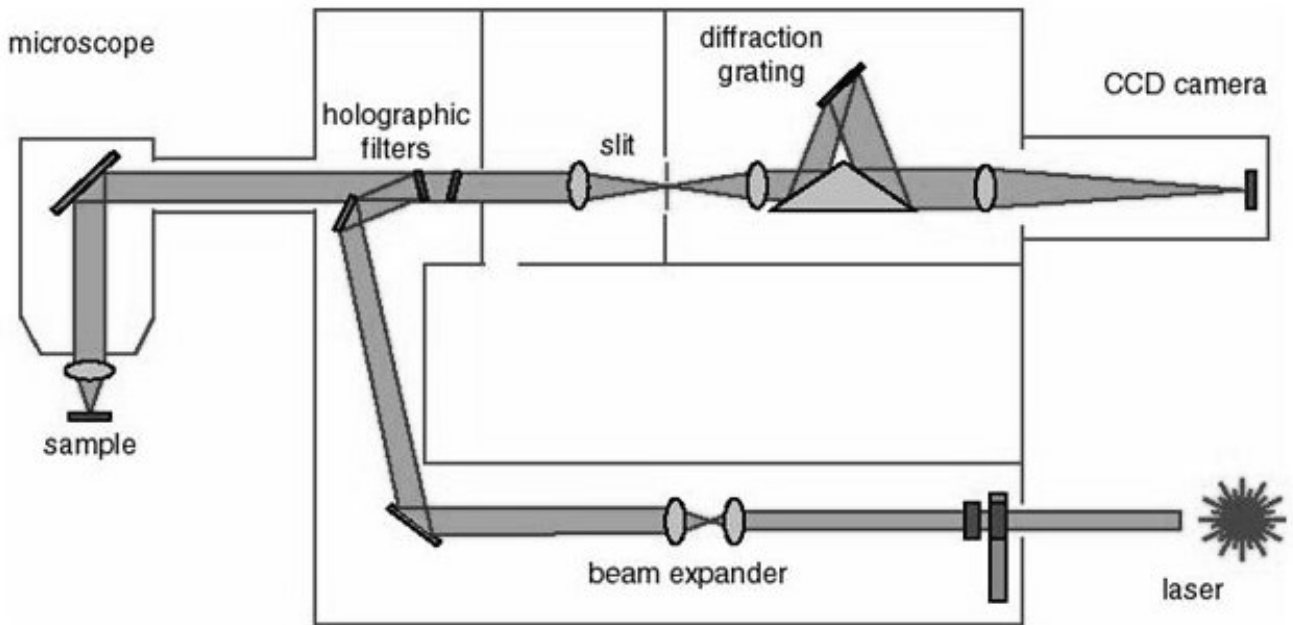
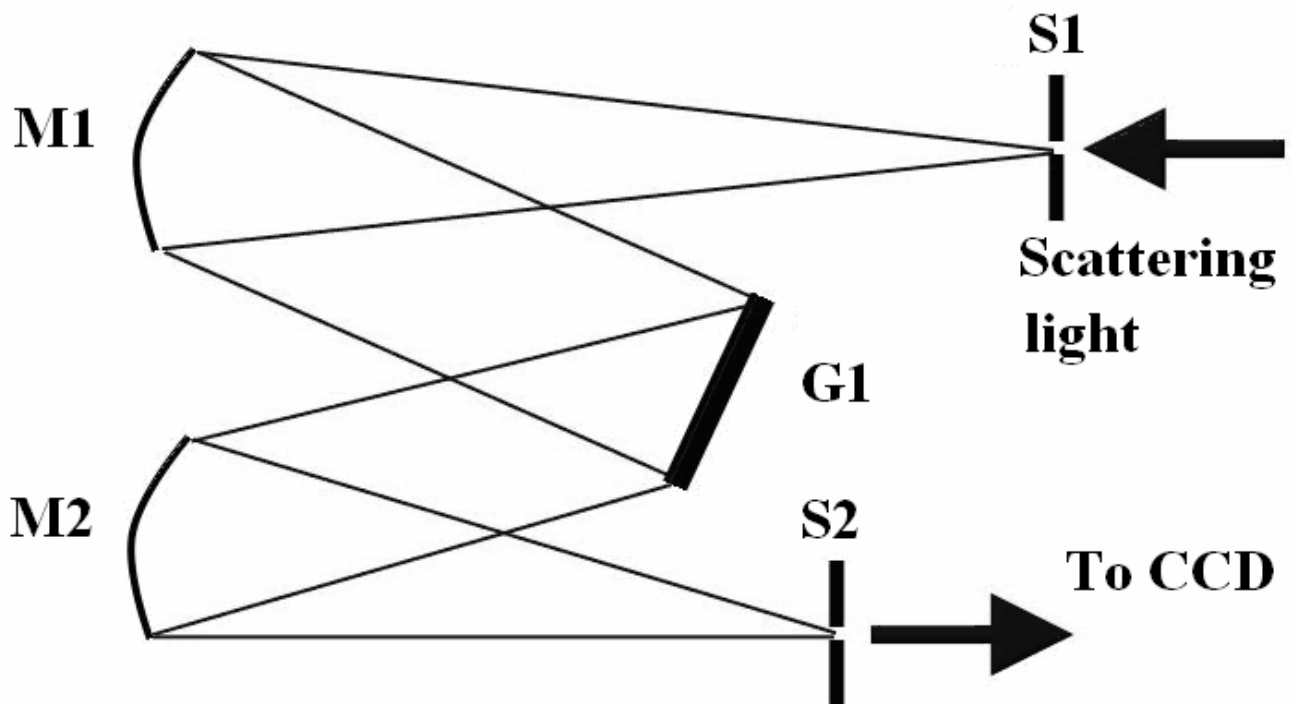Fig. 3 - 5. A sketch of the setup of the micro-Raman scattering in Tatung University.

Fig. 3 - 6. Schematic diagram of a single monochromator. G is optical grating, M is mirror, and S is slit.
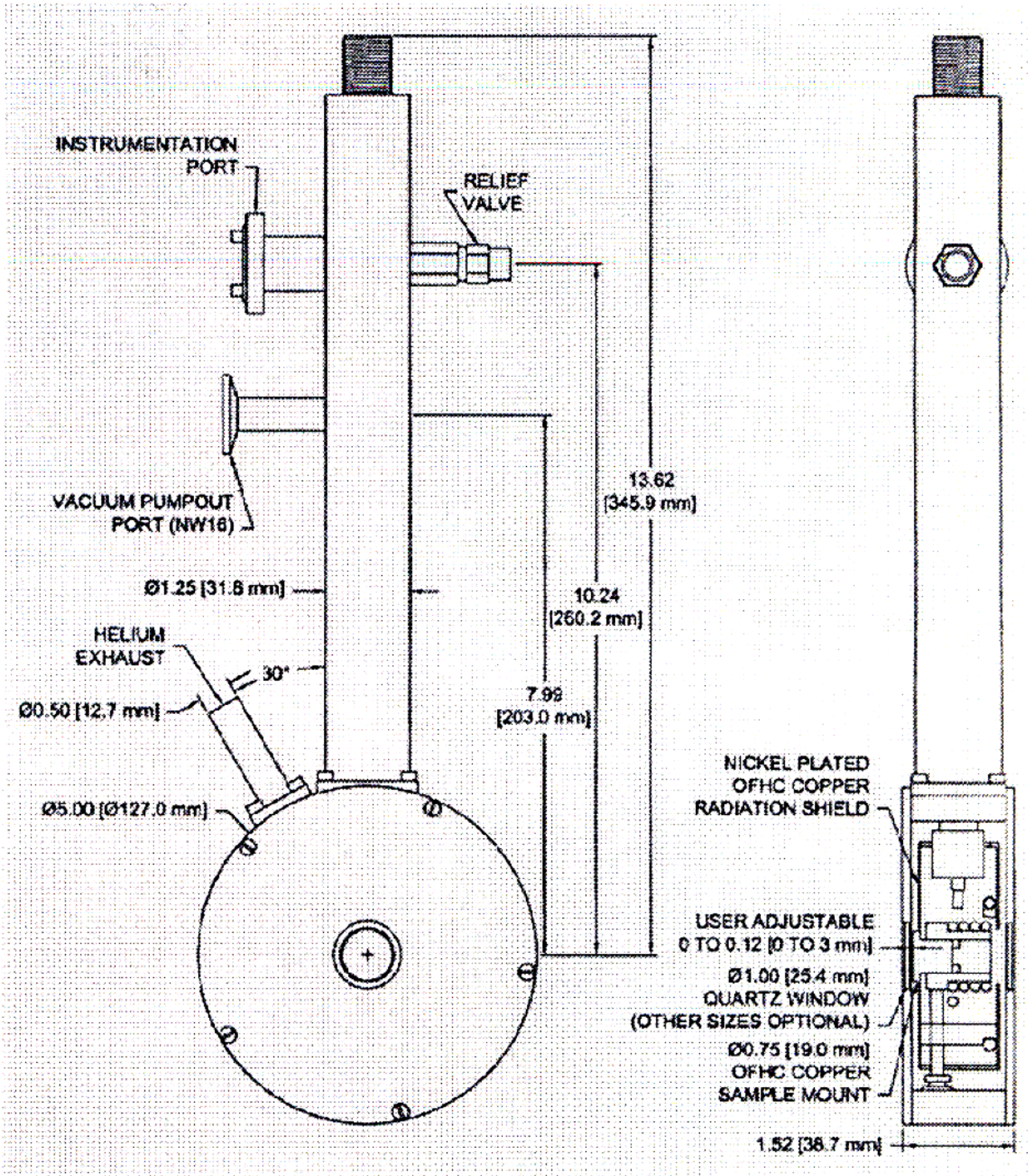
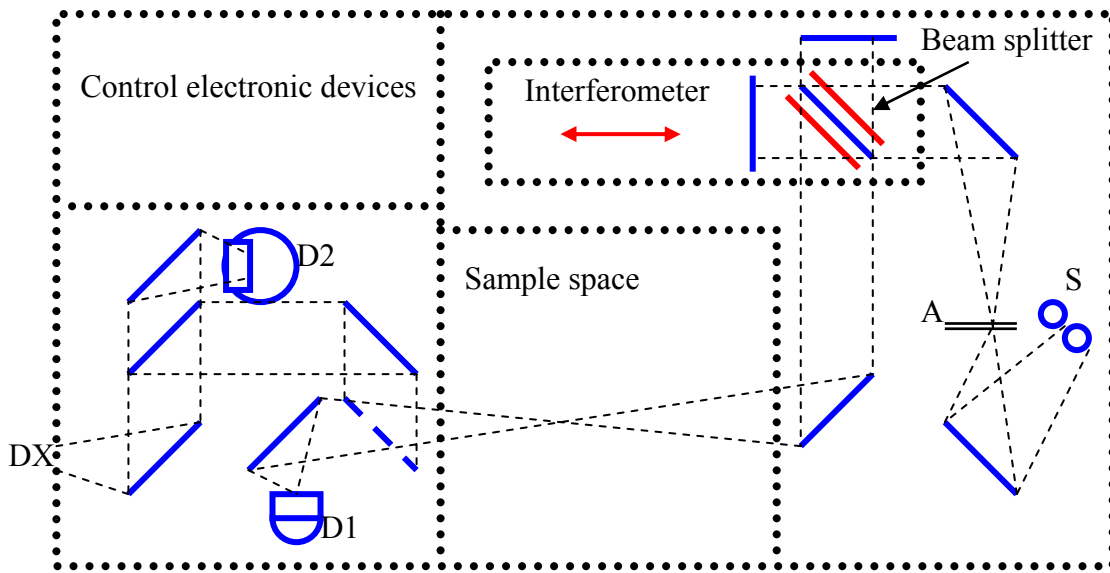Fig. 3 - 7. A sketch of cryostat which is used in temperature-dependent micro-Raman scattering.[67]

Control electronic devices

Interferometer

Beam splitter

Sample space

D2

A

S

DX

D1

Fig. 3 - 8. Experimental setup of the Fourier transform infrared spectrometer (BRUKER IFS 66v/s). (S: light sources, A: aperture, and D: detectors.)[65]
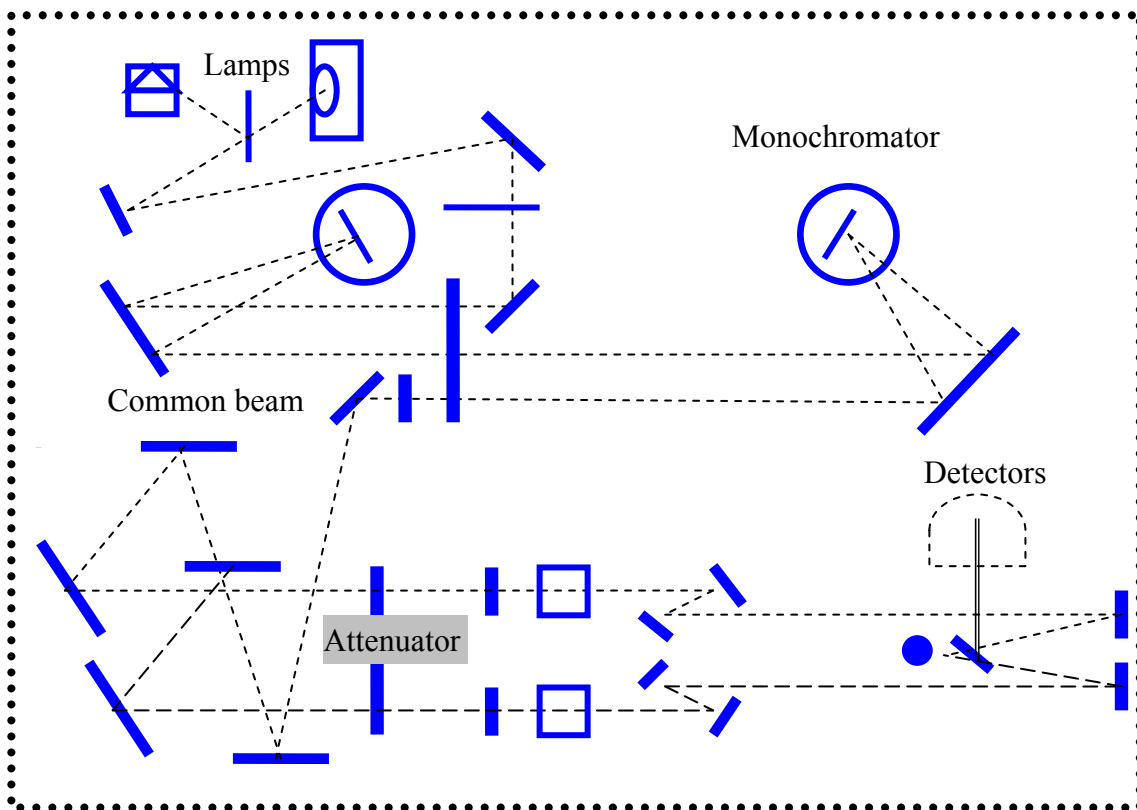
Lamps

Monochromator

Common beam

Detectors

Attenuator

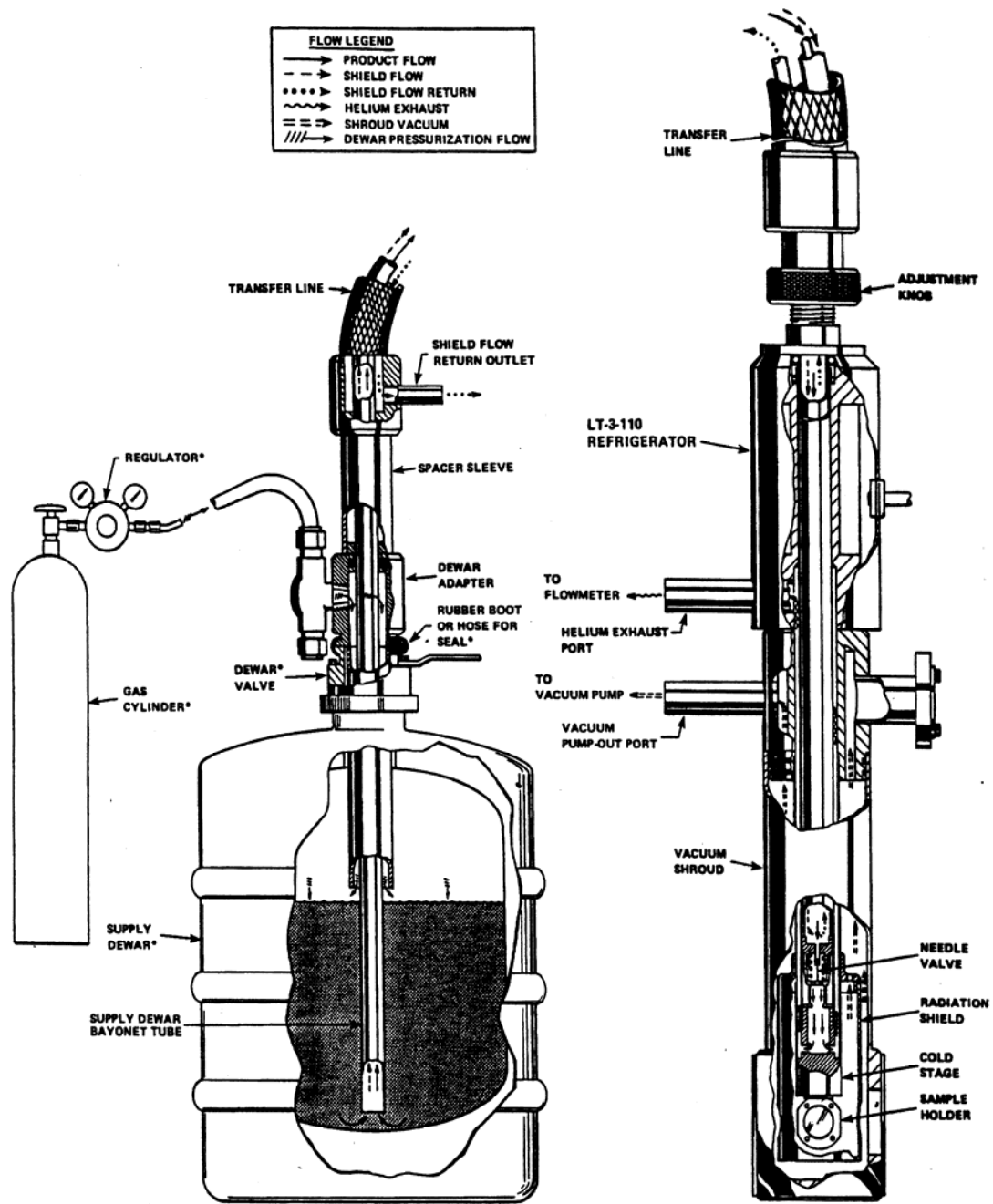Fig. 3 - 9. Experimental setup of the UV/VIS/NIR spectrometer (Perkin Elmer Lambda 900).[68]

Fig. 3 - 10. Experimental setup of cooling system.[68]